ACS Sustainable Chemistry & Engineering

pubs.acs.org/journal/ascecg

Research Article

Scale-Up Analysis of Inductively Heated Metamaterial Reactors

Chenghao Wan, Connor Cremers, Ariana B. Höfelmann, Zhennan Ru, Calvin H. Lin, Kesha N. Tamakuwala, Dorothy L. Mantle, Pinak Mohapatra, Juan Rivas-Davila, Matthew W. Kanan, and Jonathan A. Fan*

Cite This: *ACS Sustainable Chem. Eng.* 2026, 14, 5323−5331

Read Online

ACCESS | Metrics & More | Article Recommendations | Supporting Information

ABSTRACT: Inductively heated metamaterial reactors, which utilize an open-cell lattice baffle structure as a heating susceptor for electromagnetic induction, are promising candidates for scaled, electrified thermochemical reactor operation due to their ability to support volumetric, eddy-current-based heating profiles and enhanced heat transfer properties. We present a systematic scale-up analysis of inductive metamaterial reactors where we utilize a combination of analytic modeling, numerical simulations, and experiments to project the capabilities and performance of scaled reactors. The experimental metamaterial reactor consists of an open-cell SiSiC foam with electrical properties and lattice geometries that are codesigned with the induction frequency to maximize heating uniformity and coupling efficiency across different reactor scales. We use reverse water−gas shift as a model reaction system and show that for reactor configurations featuring a uniform metamaterial susceptor, the total system efficiency increases with scale. However, the throughput of these scaled reactors is limited by the radial temperature gradients. We further show that this bottleneck can be overcome by tailoring the radial effective electrical conductivity profile of the susceptor, which can enable scaled reactors with nearly ideal plug-flow-like capabilities. These concepts provide a pathway toward scaled electrified thermochemical reactors with optimal chemical conversion capabilities.

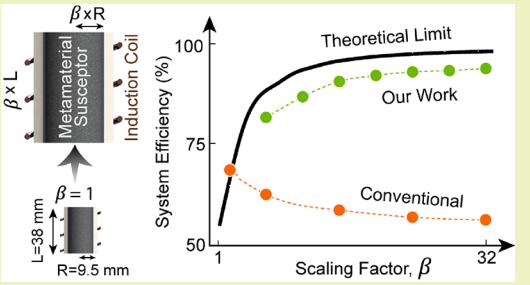

KEYWORDS: *induction heating, electrification, decarbonization, process intensification, electrified reactors, reverse water−gas shift*

INTRODUCTION

The electrification of thermochemical reactors serves as a promising route to decarbonizing chemical manufacturing processes and enhancing the capabilities of chemical reactors.[1,2] To date, proof-of-concept demonstrations of various electrified reactor heating methods have been explored, including those based on resistive Joule heating,[3−6] microwaves,[7−10] thermal plasmas,[11−14] and electromagnetic induction.[15−19] These studies have shown that electrified heating methods can support enhanced heat transfer rates to catalytic sites beyond the capabilities of fossil fuel-based heating methods, enabling the process intensification of highly endothermic reactions.[20−22] Electrified heating methods have also been shown to support the selective heating of reactants and catalysts, enhancing the selectivity and conversion of reactants to products.[23,24]

While electrified thermochemical reactors hold great promise as translational clean energy technologies, scalability remains a key challenge.[25,26] Resistive heating elements are highly efficient but typically have a form factor of one-dimensional tubes or wires that are challenging to adapt to three-dimensional volumes. Additionally, ensuring robust electrical contacts at high temperatures is nontrivial and often requires specialized materials. Microwave heating sources enable wireless and selective heating but are limited by the finite penetration depth of microwaves in typical reactor environments and inefficient power electronics. Thermal plasma heating can achieve extreme temperatures suitable for specialized reactions, such as pyrolysis, but it is difficult to adapt to mainstream catalytic systems. With these considerations in mind, electromagnetic induction heating has been identified as a particularly attractive approach to scaled electrified reactor operation because it can produce volumetric heating profiles, operates with high input voltages and low input currents due to its intrinsic transformer properties, and has been demonstrated to effectively operate at megawatt power levels.[27] Modes of induction heating include the heating of magnetic materials by hysteresis, which can enable the selective heating of magnetic catalysts,[28] and the more general heating of electrically conductive materials by eddy currents,[29] which will be the focus here.

Among the most advanced eddy-current-based inductive reactor concepts are metamaterial reactors, which we recently

Received: July 30, 2025
Revised: February 25, 2026
Accepted: February 27, 2026
Published: March 7, 2026

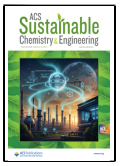

https://doi.org/10.1021/acssuschemeng.5c07929
ACS Sustainable Chem. Eng. 2026, 14, 5323−5331

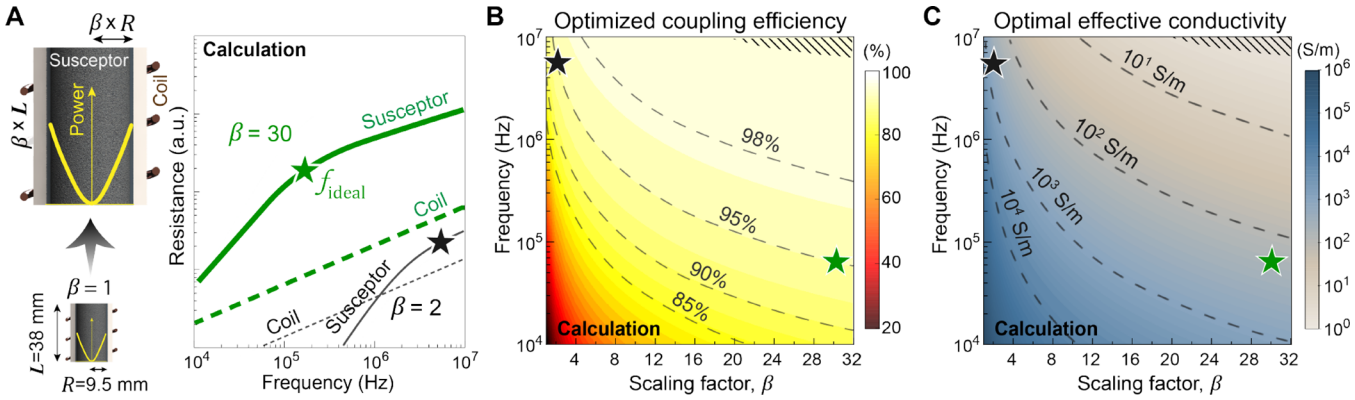

Figure 1. Optimized coupling efficiencies of scaled metamaterial reactors with optimal uniform σ_{eff}. (A) AC resistances of the susceptor (R_{susc}) and coil (R_{coil}) as a function of the induction frequency for two different reactor sizes. The R_{susc} curves feature a low-frequency, volumetric heating regime where $R_{susc} \propto f^2$ and a high-frequency, surface heating regime where $R_{susc} \propto \sqrt{f}$. The transition frequency, f_{ideal}, separates these regimes and delineates the optimal heating condition. (B) Contour plot of coupling efficiency as a function of β and operating frequency, assuming optimal heating conditions. Regions of high coupling efficiency (over 90%) are achieved at MHz frequencies for small β and at kHz frequencies for large β. (C) Contour plot of optimal σ_{eff} values corresponding to ideal heating conditions.

proposed and where an internal structured susceptor is tailored with the electromagnetic induction frequency to enable volumetric heating and high coupling efficiencies.[30] This structured susceptor functions as a reactor baffle, serving as both the inductively heated element and the structural component that supports catalyst packing. Coupling efficiency here corresponds to the fraction of electrical energy input into the induction coil that converts to heat in the susceptor. An important design consideration with metamaterial reactors is the modeling of the baffle as a homogeneous medium with effective electrical conductivity (σ_{eff}), which enables the tractable evaluation and optimization of macroscopic reactor heating properties. These induction heating concepts complement recent developments in structured reactors, where architected baffles have been proposed to enhance the heat transfer and hydrodynamic properties within a reactor.[31−34] In an initial laboratory-scale demonstration, we showed that a volumetric reactor metamaterial baffle comprising a conductive open-cell ceramic foam lattice could be packed with fixed-bed catalytic material and facilitate the reverse water−gas shift (RWGS) reaction near the thermal equilibrium conversion limits.

In this study, we investigate how the capabilities and efficiencies of inductively heated metamaterial reactors scale as the reactor size increases from laboratory to commercial scales. We specifically investigate reactor metrics as a function of β, which is a linear scaling factor for the diameter and length of the reactor and the coil pitch (Figure 1A). We consider β values ranging from 1 to 32, which corresponds to reactor radii (R) spanning 0.0094−0.3 m. We show that for reactors with uniform metamaterial baffles of constant effective electrical conductivity, the baffle electrical conductivity and induction frequency can be tailored as a function of β to enable high coupling efficiency while maintaining a volumetric parabolic heating profile. We then project the capabilities of scaled reactors with uniform baffles, using a multiphysics model fine-tuned with experimental laboratory-scale reactor data, and find that conversion and throughput are ultimately limited by radial temperature gradients. We then discuss how these radial temperature gradients can be mitigated by tailoring the radial effective electrical conductivity profile of the metamaterial susceptor, enabling scaled reactor performance with nearly ideal plug-flow-type characteristics.

EXPERIMENTS

Coupling Efficiency Scaling

We begin our analysis by briefly reviewing the heating properties and ideal operating regimes of inductive metamaterial tubular reactors with uniform cylindrical baffles. A more detailed discussion can be found in ref 30. The macroscopic heating profile is dictated by the susceptor skin depth, δ, which represents the penetration depth of the coil-generated alternating magnetic field into the susceptor. It is defined to be $\delta = \sqrt{1/(\pi\sigma_{eff} f \mu_0)}$, where f is the induction frequency and σ_{eff} is the effective electrical conductivity of the metamaterial susceptor. When δ is larger than $\sim R/2$, the heating profile is volumetric and approximately parabolic, and when δ is smaller than $\sim R/2$, the heating profile becomes confined to the outer circumferential edges of the reactor.

The total power dissipated in the susceptor relates to the susceptor AC resistance (R_{susc}), which is a function of δ, σ_{eff}, and R and has a frequency-dependent profile, as shown in Figure 1A. The induction coil itself also dissipates heat and has an AC resistance, R_{coil}. More detailed expressions of these terms are in Sections S1 and S4. At relatively low frequencies, R_{susc} scales as f^2, while R_{coil} scales as $\sqrt{f}$, and the coupling efficiency, $R_{susc}/(R_{coil} + R_{susc})$, increases with frequency.[30] At high frequencies, both R_{susc} and R_{coil} scale as $\sqrt{f}$, and the coupling efficiency is capped. The transition point between these regimes occurs at f_{ideal} when $\delta \sim R/2$. This point represents the ideal induction heating condition for a particular reactor configuration, as it features a volumetric heating profile and nearly maximal coupling efficiencies.

We utilized this understanding to probe how scaled reactor systems with uniform susceptors can operate, assuming ideal heating conditions. A contour map showing coupling efficiency for differing β and induction frequencies is shown in Figure 1B. The baffle σ_{eff} at each point on the map is adjusted to ensure ideal heating conditions, and the corresponding contour map of σ_{eff} is presented in Figure 1C. Each contour plot also includes reference lines representing constant coupling efficiency (Figure 1B) or effective electrical conductivity (Figure 1C) values, and the points from Figure 1A are also plotted as specific examples. The hatched region at the top right of the plots represents a nonoperable regime, where the induction coil itself is self-resonant and no longer operating in the quasi-magnetostatic limit, setting frequency limits in scaled systems (see Section S4 for more discussion). The boundary of this region is conservatively specified, as

https://doi.org/10.1021/acssuschemeng.5c07929
ACS Sustainable Chem. Eng. 2026, 14, 5323−5331

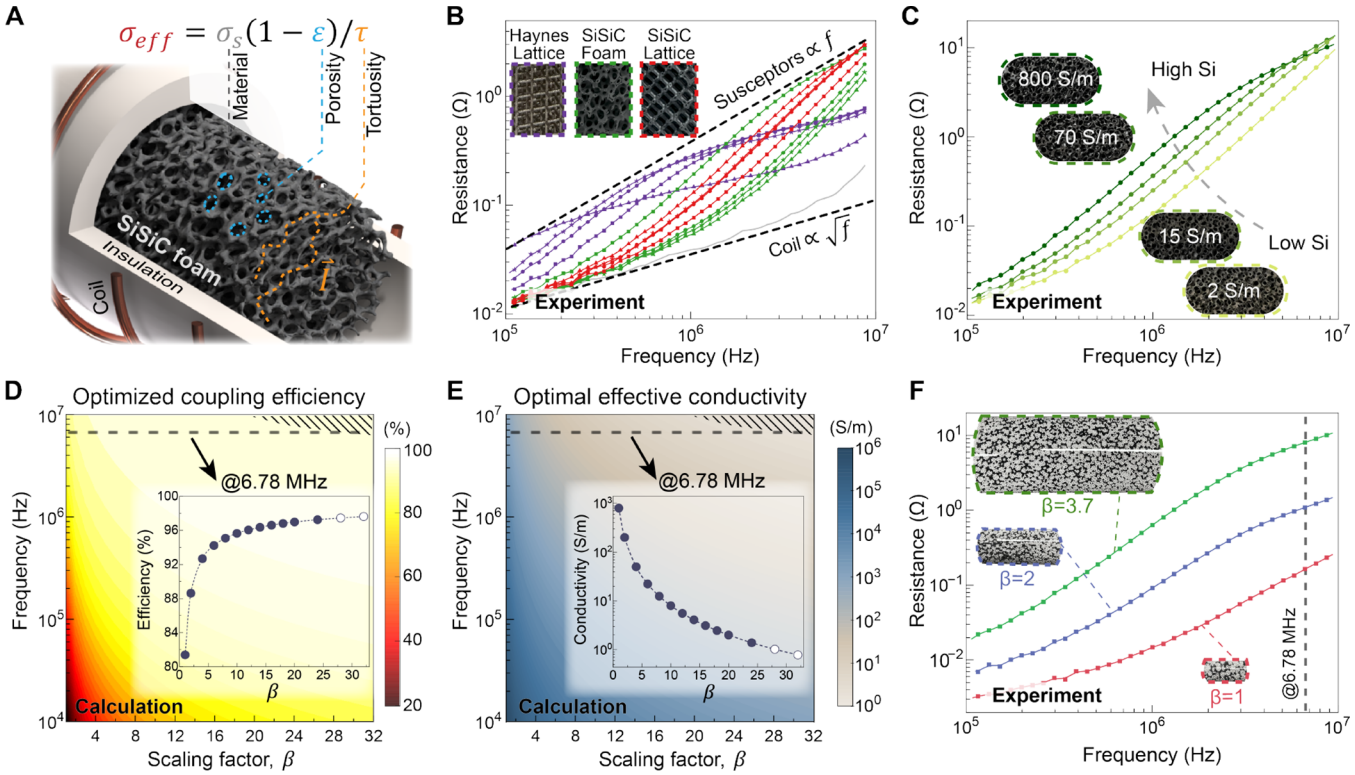

Figure 2. Effective electrical conductivity properties of uniform metamaterial susceptors. (A) Schematic of a metamaterial reactor comprising an open-cell lattice susceptor that is inductively heated with a helical induction coil. The susceptor effective electrical conductivity is specified by the Lemlich limit and is a function of the material and geometric lattice parameters. (B) Experimental impedance measurements of different cylindrical metamaterial susceptors. Insets show images of foam and cubic lattice susceptors comprising the Haynes superalloy and SiSiC. (C) Impedance characterization of 75 mm-diameter SiSiC foam susceptors with different silicon loadings, showing effective electrical conductivities ranging from 2 to 800 S/m. (D) Coupling efficiency vs β at a fixed induction frequency of 6.78 MHz. As β increases, the efficiency approaches 100%. (E) σ_{eff} tuning required for the scaling trend shown in (D). (F) Impedance measurements of susceptors with β = 1, 2, and 3.7, each with tuned σ_{eff} such that $f_{ideal} \sim$ 6.78 MHz. The insets are images of the catalyst-packed susceptors.

parasitics in the coil system can practically lead to a larger nonoperable regime in scaled systems.

For small reactors, coupling efficiencies greater than 90% are possible only at megahertz frequencies. As the reactor scales and coupling efficiency is maintained constant, f follows the reference lines and reduces to values below one megahertz (Figure 1B), during which σ_{eff} remains nearly constant (Figure 1C). The ability of scaled reactor systems to operate with high coupling efficiencies and with f in the kilohertz range is important from the standpoint of power electronics. Megahertz-frequency induction requires the use of high-frequency power electronics based on wide-bandgap switches and resonant power amplifier topologies, which have limited power output and are best suited for laboratory- and pilot-scale reactors. At kilohertz frequencies, our scaled reactor systems can utilize silicon-based power electronics, which are a more mature technology, can support higher power levels, and can convert DC to AC power with near-unity efficiency.[35]

The range of susceptor σ_{eff} values required for different scaled system configurations necessitates a customizable susceptor platform for tuning σ_{eff}. We show experimentally that σ_{eff} can be widely tuned by tailoring the geometry and composition of the susceptor, and that this tuning can be accurately characterized using an effective-medium picture described by the Lemlich limit,[36] which provides a simple expression relating σ_{eff} to the baffle material electrical conductivity, lattice porosity, and lattice tortuosity (Figure 2A). To demonstrate, we perform AC resistance measurements on open-cell lattice susceptors with the same cylindrical geometry (38 mm diameter, 150 mm length) but made from different high-temperature-stable materials (Haynes superalloy metal and reaction-bonded silicon carbide, i.e., SiSiC), different lattice types (random foams and cubic lattices made by additive manufacturing), and porosity values ranging from 0.8 to 0.99. The resistance curves are plotted in Figure 2B and show that the impedance curves all have AC resistance values that initially scale as f^2 followed by $\sqrt{f}$, which are the same trends featured in Figure 1A for homogeneous media. Furthermore, the f_{ideal} of the curves spans frequencies ranging over 2 orders of magnitude, and they lie on a trend line proportional to frequency, which follows the theory for homogeneous conductive cylinder induction heating.[30] We note that the lattice susceptors measured in Figure 2 have an aspect ratio (length-to-radius) of approximately 8, which differs from the aspect ratio of 4 used in other experiments and scale-up analysis. This difference does not influence the location of f_{ideal}, which corresponds to the condition in which the skin depth equals half of the susceptor radius and is therefore independent of the susceptor length.

SiSiC, which will be the focus of the rest of this study, is particularly ideal for scaled reactor implementation because of its chemical inertness, high-temperature compatibility, low thermal expansion, and high thermal conductivity.[37] In addition, its material electrical conductivity can be tuned by adjusting its silicon content during manufacturing.[38,39] To explore the extent of this tuning mechanism, we characterize cylindrical SiSiC foams (70 mm diameter) with consistent geometric parameters but made with different amounts of silicon loading. The resulting resistance curves are shown in Figure 2C, and curve fitting yields σ_{eff} values ranging from 2 to 800 S/m. This ability to tune effective electrical conductivity is particularly important for operating scaled high-frequency reactors. To demonstrate, we fix induction frequency to 6.78 MHz, which is a dedicated frequency in the electromagnetic industrial, scientific, and medical band,[40] and increase β. We see in Figure 2D that as β increases, the calculated coupling efficiency increases and approaches 100%. The

https://doi.org/10.1021/acssuschemeng.5c07929
ACS Sustainable Chem. Eng. 2026, 14, 5323−5331

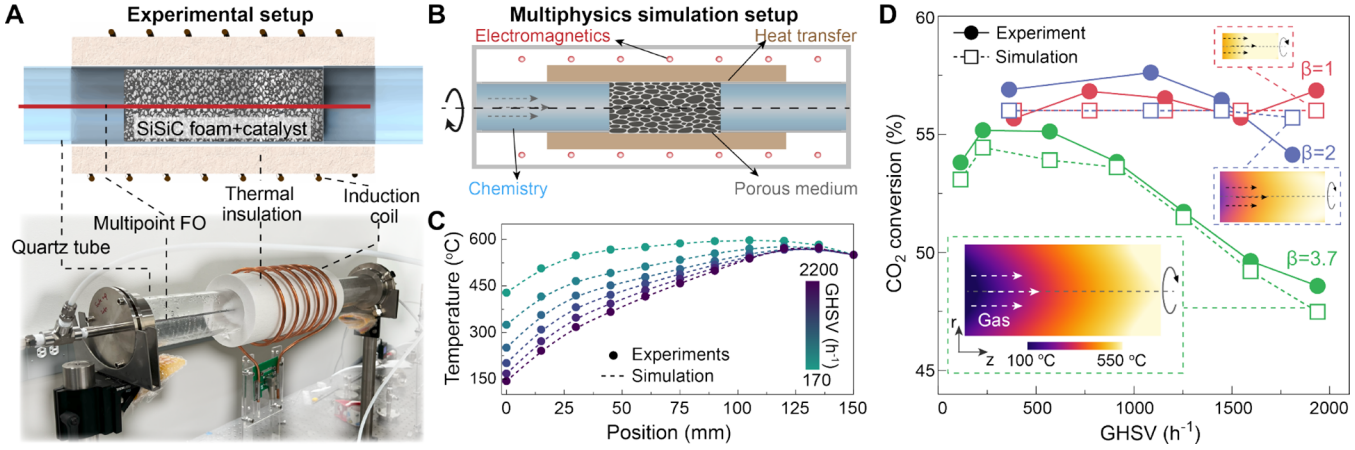

Figure 3. Experimentally refined multiphysics reactor model. (A) Cross-sectional schematic (top) and image (bottom) of the experimental metamaterial reactor setup. (B) Schematic of our multiphysics modeling effort, which combines electromagnetics, heat transfer, fluid flow, and chemical reaction modalities. (C) Experimental axial temperature profiles across different GHSV conditions (solid circles) and corresponding simulated profiles (dashed lines) are fitted using our multiphysics reactor model to the experimental profiles. (D) CO_2 conversion as a function of GHSV for three reactor sizes, measured experimentally (solid circles) and simulated (open squares) using our fitted multiphysics model from panel (C). The experimental and simulated conversions agree well for all cases. The insets are simulated 2D temperature profiles of the reactors at high GHSV values.

required σ_{eff} scales as approximately $1/\sqrt{\beta}$ (Figure 2E). This scaling regime can be captured experimentally, and we characterize a set of SiSiC foam susceptors representing different β values (1, 2, and 3.7) with a tuned σ_{eff}. The AC resistance curves (Figure 2F) each show an f_{ideal} at approximately 6.78 MHz, and fits of these curves with our AC resistance model yield σ_{eff} values of 400, 201, and 70 S/m for β = 1, 2, and 3.7, respectively. The AC resistance scales proportional to the reactor volume (i.e., β^3) at this frequency, which matches our analytic derivation (Supplementary S1) and our previous work.[30]

Total Efficiency Scaling

A more comprehensive performance assessment of the total efficiency of scaled metamaterial reactors requires an analysis of heat utilization, heat loss, and temperature profiling within the reactor itself. We define total efficiency to be the ratio of energy used to heat the inlet gas and drive the endothermic reaction divided by the electrical energy input into the power electronics. In particular, losses arise from heat loss to the environment, resistive loss in the induction coil, and inefficiencies in the power electronics. To perform this analysis, we consider the RWGS reaction as our model chemical system for the study. The RWGS reaction is an endothermic reaction that converts CO_2 and H_2 into CO and $_{H2O}$, and it has been explored as a foundational reaction for the circular carbon economy due to its utilization of carbon dioxide.[41] We first perform experiments with laboratory-scale reactors of different sizes (Figure 3A) and match the reactor characteristics with multiphysics simulations (Figure 3B) to produce an experimentally refined reactor model. We then extrapolate this refined model to investigate the performance of larger reactors. The laboratory-scale reactors used for experimental study utilize the susceptors shown in Figure 2F. The RWGS catalyst consists of 18 wt % K_2CO_3 on 1 mm-diameter mesoporous Al_2O_3 supports, and it is chosen because it features high activity at moderate temperatures (≥430 °C), 100% selectivity for CO with no CH_4 byproduct, and excellent multiday stability.[42,43] We note that the catalyst particles do not couple to the electromagnetic field and that catalyst heating occurs solely through conductive heat transfer from the structured SiSiC susceptor. In addition, under RWGS conditions with high CO_2 partial pressure, K_2CO_3 largely retains its carbonate form and exhibits well-documented high CO-selective activity, consistent with prior reports.[43]

A schematic and photograph of the experimental setup (Figure 3A) show a susceptor baffle that is packed with catalyst particles and housed within a quartz tube. It is further surrounded by 25 mm-thick aluminosilicate thermal insulation and is heated using a helical induction coil. To maintain a uniform magnetic field across the susceptor, the induction coil length was chosen to extend slightly beyond both ends of the susceptor (see Supporting Information for details). A multipoint fiber-optic (FO) temperature sensor placed along the rotational symmetry axis is used to fix the outlet temperature to 550 °C by providing feedback to the coil power supply, and it also simultaneously monitors the axial temperature profile within the reactor. An FO sensor is used over a thermocouple due to its insensitivity to magnetic fields, ensuring accurate measurements during induction heating. We run RWGS reactions using this configuration for the three susceptor sizes and gas hourly space velocity (GHSV) values of up to 1800 h^{-1}. The reported GHSV values are calculated based on the total bed volume (susceptor + catalyst + void), of which the catalyst constitutes only 46%. The GHSV values are relatively low due to the atmospheric pressure operation and the catalyst form-factor used in this study. We note that the same catalyst in powder form has been previously demonstrated to achieve equilibrium conversion at GHSV values of 30,000 h^{-1} and 10 bar pressure at T > 500 °C, which differentiates it from transition-metal-based catalysts that are prone to methane and coke formation at intermediate temperatures and elevated pressures.[43] Experimental axial temperature profiles are shown in Figure 3C, and experimental CO_2 conversion (X_{CO_2}) results are shown as solid dots in Figure 3D. For the β = 1 and 2 reactors, conversion values are near equilibrium values over the tested GHSV range. However, for the β = 3.7 reactor, conversion begins to deviate at higher GHSV values, suggesting a breakdown of plug-flow-like reactor behavior.

Our experimentally refined reactor model uses COMSOL Multiphysics and considers the induction heating process, heat transfer, fluid flow, and reaction enthalpy in our model. To perform these multiphysics simulations, we first perform electromagnetic simulations to compute the induction heating profile within the susceptor. The electromagnetic properties of SiSiC are effectively independent of temperature, enabling the heating profile to be calculated independently of other physical parameters. This profile is then input into a coupled heat-transfer and reaction simulator in which heat transfer processes and heat consumption from the reaction are iteratively solved until self-consistency. For these simulations, we assume that the packed-bed reaction zone consists of a porous medium that is described using the Brinkman equation[44] and that has a void fraction of 0.5. The catalyst reaction kinetics and the thermal conductivity of the reactor materials outside the reaction zone are taken from our prior study.[30] Experimental model refinement is performed for the thermal conductivity of the reaction zone, which is

https://doi.org/10.1021/acssuschemeng.5c07929
ACS Sustainable Chem. Eng. 2026, 14, 5323−5331

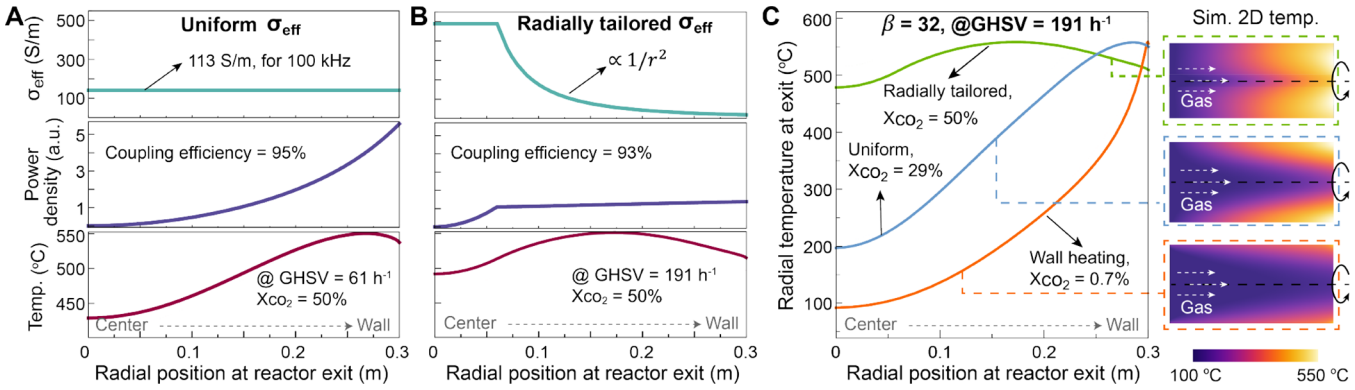

Figure 4. Radial tailoring of metamaterial susceptor effective electrical conductivity. (A, B) Effective electrical conductivity profile (top panel), heat dissipation profile (middle panel), and radial temperature profile at the outlet (bottom panel) for a (A) uniform and (B) a radially tailored metamaterial reactor. Both reactors have a 0.6 m diameter (β = 32), operate with a 100 kHz frequency, have a maximum internal temperature of 550 °C, and have a fixed CO_2 conversion of 50%. The uniform susceptor features a parabolic heating profile, which leads to strong radial temperature gradients and a GHSV of 61 h^{-1}. The radially tailored susceptor features a nearly uniform volumetric heating profile, which leads to reduced radial temperature gradients and a >3-fold increase in GHSV. (C) Radial outlet temperature profiles, conversion, and axial temperature profiles of wall-heated, uniform metamaterial, and radially tailored metamaterial reactors. GHSV is fixed at 197 h^{-1} and β = 32 in all cases.

extracted by fitting the model to the experimental axial temperature profiles (Figure 3C), and is determined to be 11 W/(K·m).

The calculated CO_2 conversion rates from our refined model are shown as open dots in Figure 3D and agree well with our experimental data. The observed trends in CO_2 conversion can be further analyzed by calculating the full temperature profile within the reactor systems at high flow rates for different β values, which are shown as insets in Figure 3D. For β = 1 and 2, the temperature profile supports small radial temperature gradients, indicating that the system operates near plug-flow-like behavior due to the small dimensions of the system. For β = 3.7, on the other hand, there are significant radial temperature gradients that are responsible for the observed drop in CO_2 conversion. As such, while uniform metamaterial reactors attempt to manage radial temperature gradients by use of a volumetric heating profile and a high internal thermal conductivity, nontrivial gradients still persist for β greater than 2.

RESULTS AND DISCUSSION

To mitigate radial temperature gradients in scaled metamaterial reactors, we leverage one of the distinguishing features of metamaterial reactors: the ability to spatially tailor the heating profile through control of the local effective electrical conductivity. In particular, spatially varying effective electrical conductivity profiles can be achieved by spatially modifying the local susceptor geometry and material composition (Figure 2). To demonstrate this, we consider a metamaterial susceptor with an electrical conductivity profile that follows $1/r^2$, which explicitly supports a volumetrically uniform heating profile when heated with a uniform axial magnetic field (Section S3). In practice, it is not possible to specify this exact profile due to the divergence in electrical conductivity at the rotational symmetry axis of the cylinder, and we instead consider the following effective electrical conductivity profile:

$$\sigma(r) = \begin{cases} \dfrac{\sigma_{\text{eff}}}{A}\cdot\left(\dfrac{R}{r}\right)^2, & \text{for } R/5 < r \le R \\ \dfrac{\sigma_{\text{eff}} \times 25}{A}, & \text{for } 0 \le r \le R/5 \end{cases} \quad (1)$$

where σ_{eff} is the corresponding effective electrical conductivity chosen for the homogeneous susceptor, and A is a hyperparameter used to scale the magnitude of the parabolic radial electrical conductivity profile and is swept (Figure S3A) to identify the value of 600 that yields optimal heating uniformity and coupling efficiency.

To examine the impact of radial susceptor customization on reactor performance, we simulate the performance of scaled uniform and radially dependent metamaterial reactors utilizing our experimentally refined model for β = 32. Plots of the effective electrical conductivity profiles, heating profiles, and radial temperature distributions for uniform and radially tailored reactors are shown in Figure 4A,B, respectively. In both cases, the maximum temperature in the reactor is set to 550 °C, and the GHSV is chosen such that the conversion of carbon dioxide is 50%. In addition, the induction frequency is chosen to be 100 kHz, which corresponds to the 95% coupling efficiency contour line for homogeneous susceptors in Figure 1B.

The heating profile for the uniform susceptor features a parabolic-like radial heating profile (middle panel, Figure 4A), which is consistent with the volumetric heating profile in uniform cylindrical susceptors with helical coils at all scales. The underheated center region leads to significant radial temperature gradients at the outlet (bottom panel, Figure 4A) that limit the GHSV to 61 h^{-1}, indicating that relatively long residence times are required to achieve our desired conversion. Our radially tailored reactor supports a nearly uniform heating profile (middle panel, Figure 4B) while operating with a nearly identical coupling efficiency. The corresponding radial temperature profile at the outlet (bottom panel, Figure 4B) is much more uniform, though radial temperature gradients still persist due to heat loss through the thermal insulation and the lack of heating at the central region along the axis of the cylindrical reactor. These reactors support a GHSV of 197 h^{-1}, which is more than threefold higher than for the uniform case and which shows how radial tailoring can enable process intensification and the use of larger reactant flows.

To further evaluate the impact of radial tailoring on scaled reactor performance, we compare the capabilities of scaled uniform metamaterial reactors, radially tailored metamaterial reactors, and wall-heated reactors under the same GHSV of 197 h^{-1} and a maximum reactor temperature of 550 °C. The wall-heated reactor also contains a SiSiC foam to enhance its internal thermal conductivity and improve heat spreading in the reactor. The radial temperature profiles at the outlet for all

https://doi.org/10.1021/acssuschemeng.5c07929
ACS Sustainable Chem. Eng. 2026, 14, 5323−5331

cases are shown in Figure 4C. The wall-heated reactor, which is included as a simple reference, exhibits extreme temperature gradients and displays nearly no conversion. The homogeneous metamaterial reactor also displays strong radial temperature gradients spanning hundreds of degrees that result in a conversion of 29%. The radially tailored reactor, on the other hand, has a conversion of 50%, which is near the equilibrium conversion value of 55%. Cross-sectional temperature plots of the reactors show that radial temperature gradients at all axial positions of the reactor are significantly reduced with the radial-tailored metamaterial approach.

Finally, we perform a systematic analysis of scaled metamaterial reactor performance for β = 4−32. We consider uniform and radially tailored metamaterial reactors and wall-heated reactors with SiSiC baffles. Our analysis can ultimately extend to larger β without loss of generality, though we view moderate-scale metamaterial reactors as representative of commercial-scale systems due to the ability of metamaterial reactors to intensify highly endothermic reactions and support enhanced product throughput. For all scales and reactor types, we set the induction frequency to follow the 95% coupling efficiency contour line in Figure 1B. We assume that the efficiency of the power electronics itself is 95%, which is consistent with reported efficiencies of wide-bandgap-based amplifiers at megahertz frequencies and silicon-based amplifiers at kilohertz frequencies.[35] The effective electrical conductivity values and profiles of the metamaterial susceptors are optimized for coupling efficiency for each β value and susceptor type. A summary of chosen reactor parameters for different β values is given in Table 1, along with the two

Table 1. Simulation Parameters for Scale-Up Analysis

			susceptor conductivity		dimensionless parameters	
β	susceptor diameter (m)	frequency (MHz)	σ_{eff} (homo) (S/m)	A for $\sigma(r)$ in eq 1	Re	Da
4	0.075	3	240.4	N/A	1.25	15.1
8	0.15	0.93	193.4	14.06	1.37	26
16	0.3	0.3	150	11.25	1.47	37.2
20	0.375	0.21	137.5	10.55	1.6	47.5
24	0.45	0.16	127.7	10.13	1.67	57.7
28	0.525	0.12	119.9	8.27	1.81	64.9
32	0.6	0.1	113.4	7.2	1.9	69.1

relevant dimensionless quantities, the Reynolds (Re) and Damköhler (Da) numbers. The Re values are all <10 across the reactor scales, confirming that the flow remains in the laminar regime. The Da values are all much greater than 1, indicating that the observed decrease in the level of CO_2 conversion at high flow rates (Figure 3D) arises from limited residence time rather than kinetic limitations. Additional details of these calculations and our experimental and simulation setup are provided in Sections S5 and S6.

We first use multiphysics simulations to determine the GHSV for each reactor type and size, in which the maximum outlet temperature is 550 °C and the corresponding CO_2 conversion is 50%. Based on the GHSV values, we calculated the corresponding space time yield (STY) values, which directly quantify reactor productivity and are reported in Figure 5A. The uniform metamaterial reactor (blue curve, Figure 5A) shows an order-of-magnitude STY enhancement for larger reactors compared to the wall-heated reactor (orange curve, Figure 5A), and the radially tailored reactor (green curve, Figure 5A) yields an additional few-fold STY enhancement over the uniform reactor. These results demonstrate that while structured reactor concepts that combine wall heating with high-thermal-conductivity baffles have some efficacy, volumetrically heated metamaterial susceptors provide a qualitatively different and better capability for $\beta \geq 8$. Furthermore, while uniform and radially tailored reactors both support volumetric heating, the uniform volumetric heating provided by radial tailoring leads to an enhanced performance for $\beta \geq 12$.

We next evaluated the total efficiency of the reactors as a function of β, assuming operation conditions from Figure 5A, and the results are plotted in Figure 5B. The black curve represents system efficiencies assuming ideal plug-flow behavior, and it serves as a theoretical limit for fixed-bed reactor operation. In this limit, the energy used to heat the gas and drive the endothermic reaction scales as β^3 and dominates in larger systems, eventually approaching the cap set by power electronics losses and coupling efficiency.[30] The uniform metamaterial reactor has an overall efficiency that increases as a function of β, indicating that while its GHSV decreases with increasing reactor size, the scaling in energy used for gas heating and the reaction follows a power law that is greater than that for parasitic losses. The radially tailored metamaterial reactor has overall efficiencies that closely follow those predicted by the plug-flow limit, highlighting the promise of spatially engineered metamaterial susceptors in addressing scale-up challenges associated with nonuniform radial temperature distributions.

CONCLUSIONS

In summary, we present a scale-up analysis of inductively heated metamaterial reactors. We utilize a combination of experimental and multiphysics analyses to elucidate how the induction frequency and susceptor electrical conductivity in uniform metamaterial reactors can be tailored to support the optimal performance in scaled systems. While these reactors can be designed to feature high coupling efficiencies, radial temperature gradients ultimately limit the process intensification capabilities and total efficiencies in scaled systems. We further propose the use of metamaterial susceptors with radially tailored effective electrical conductivity profiles that explicitly support uniform volumetric heating profiles. We show that scaled reactor systems with these susceptors have plug-flow-like chemical conversion capabilities and total efficiencies that are limited only by power electronics and coil coupling. We note that while SiSiC foams are suitable for our laboratory-scale demonstrations, they may be costly or impractical to use at larger scales due to limits in manufacturing and mechanical brittleness. However, our analysis (Figure 1C) shows that large-scale reactors can operate at lower induction frequencies with higher effective electrical conductivities (10^3−10^4 S/m), a regime where robust metal-based lattices can be manufactured and utilized.

We envision multiple pathways for future study. One direction involves a more comprehensive investigation of spatially varying metamaterial profiles in scaled systems. While we discussed in this study effective electrical conductivity profiles that support uniform volumetric heating, more complex profiles can be inversely designed to enable further enhancements in temperature uniformity in scaled systems. These concepts can also extend to axial temperature

https://doi.org/10.1021/acssuschemeng.5c07929
ACS Sustainable Chem. Eng. 2026, 14, 5323−5331

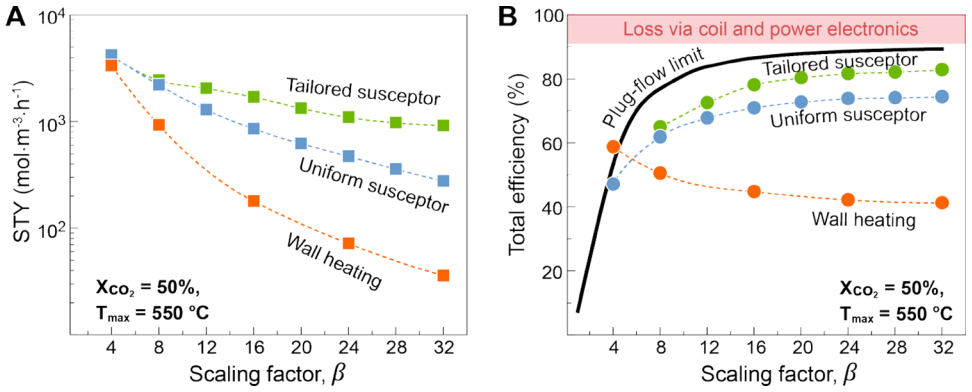

Figure 5. Process intensification and total efficiency metrics of metamaterial reactors for $\beta = 4-32$. (A) Plot of STY values corresponding to reach 50% CO_2 conversion for wall-heated, uniform metamaterial, and radially tailored metamaterial reactors of different scales. The maximum outlet temperature is fixed to 550 °C. (B) Plot of total efficiencies of the three reactors in panel (A) as a function of β, together with the efficiencies from an ideal plug-flow reactor. The radially tailored metamaterial reactor closely follows the plug-flow trend line and outperforms the other designs at scale.

customization to push the process intensification to even more extreme limits. In another direction, a more detailed analysis and understanding of power electronics efficiency and scaling are required to more comprehensively understand the capabilities and performance limits of scaled electrified reactor systems. We also envision ample opportunities to understand how scaled metamaterial susceptors with desired properties can be effectively realized by using industrially established manufacturing methods.

■ ASSOCIATED CONTENT

Supporting Information

The Supporting Information is available free of charge at https://pubs.acs.org/doi/10.1021/acssuschemeng.5c07929.

> Calculation of power dissipation and coupling efficiency; evolution of radial temperature gradients during scale-up of homogeneous susceptors; radially tailoring of the heating profile; estimation of self-resonant frequency of the induction coil; supplementary information of our experimental RWGS reactor; supplementary information of our numerical simulation; and experimental characterization of radial temperature gradient (PDF)

■ AUTHOR INFORMATION

Corresponding Author

Jonathan A. Fan − *Department of Electrical Engineering, Stanford University, Stanford, California 94305, United States;* orcid.org/0000-0001-9816-9979; Email: jonfan@stanford.edu

Authors

Chenghao Wan − *Department of Electrical Engineering, Stanford University, Stanford, California 94305, United States;* orcid.org/0000-0002-4132-4779

Connor Cremers − *Department of Electrical Engineering, Stanford University, Stanford, California 94305, United States*

Ariana B. Höfelmann − *Department of Electrical Engineering, Stanford University, Stanford, California 94305, United States*

Zhennan Ru − *Department of Materials Science and Engineering, Stanford University, Stanford, California 94305, United States*

Calvin H. Lin − *Department of Electrical Engineering, Stanford University, Stanford, California 94305, United States*

Kesha N. Tamakuwala − *Department of Chemistry, Stanford University, Stanford, California 94305, United States;* orcid.org/0000-0002-9948-0643

Dorothy L. Mantle − *Department of Mechanical Engineering, Stanford University, Stanford, California 94305, United States;* orcid.org/0009-0007-8147-3684

Pinak Mohapatra − *Department of Electrical Engineering, Stanford University, Stanford, California 94305, United States*

Juan Rivas-Davila − *Department of Electrical Engineering, Stanford University, Stanford, California 94305, United States*

Matthew W. Kanan − *Department of Chemistry, Stanford University, Stanford, California 94305, United States;* orcid.org/0000-0002-5932-6289

Complete contact information is available at: https://pubs.acs.org/10.1021/acssuschemeng.5c07929

Notes

The authors declare no competing financial interest.

■ ACKNOWLEDGMENTS

J.A.F., M.W.K., and J.R.-D. acknowledge support from the Department of Energy under agreement number DE-EE0011191. J.A.F. acknowledges support from EPIXC under agreement number M2505270. A.B.H. and C.H.L. acknowledge support from the Stanford Graduate Fellowship, and D.L.M. acknowledges support from the TomKat Graduate Fellowship.

■ REFERENCES

(1) Thiel, G. P.; Stark, A. K. To decarbonize industry, we must decarbonize heat. *Joule* **2021**, *5*, 531−550.

(2) Van Geem, K. M.; Galvita, V. V.; Marin, G. B. Making chemicals with electricity. *Science* **2019**, *364*, 734−735.

(3) Badakhsh, A.; Kwak, Y.; Lee, Y.-J.; Jeong, H.; Kim, Y.; Sohn, H.; Nam, S. W.; Yoon, C. W.; Park, C. W.; Jo, Y. S. A compact catalytic

foam reactor for decomposition of ammonia by the Joule-heating mechanism. *Chemical Engineering Journal* **2021**, *426*, No. 130802.
(4) Dong, Q.; et al. Depolymerization of plastics by means of electrified spatiotemporal heating. *Nature* **2023**, *616*, 488−494.
(5) Wismann, S. T.; Engbæk, J. S.; Vendelbo, S. B.; Bendixen, F. B.; Eriksen, W. L.; Aasberg-Petersen, K.; Frandsen, C.; Chorkendorff, I.; Mortensen, P. M. Electrified methane reforming: A compact approach to greener industrial hydrogen production. *Science* **2019**, *364*, 756−759.
(6) From, T. N.; Partoont, B.; Rautenbach, M.; Østberg, M.; Bentien, A.; Aasberg-Petersen, K.; Mortensen, P. M. Electrified steam methane reforming of biogas for sustainable syngas manufacturing and next-generation of plant design: A pilot plant study. *Chem. Eng. J.* **2024**, *479*, No. 147205.
(7) Hou, L.; Zhen, X.; Liu, L.; Kuang, D.; Gao, Y.; Luo, H.; Deng, L.; Chen, C.; Wang, S. Synthesis, thermal stability, magnetic properties, and microwave absorption applications of CoNi-C core-shell nanoparticles with tunable Co/Ni molar ratio. *Results in Physics* **2021**, *22*, No. 103893.
(8) Kappe, C. O.; Pieber, B.; Dallinger, D. Microwave Effects in Organic Synthesis: Myth or Reality? *Angew. Chem., Int. Ed.* **2013**, *52*, 1088−1094.
(9) Baker-Fales, M.; Chen, T.-Y.; Vlachos, D. G. Scale-up of microwave-assisted, continuous flow, liquid phase reactors: Application to 5-Hydroxymethylfurfural production. *Chemical Engineering Journal* **2023**, *454*, No. 139985.
(10) Sundaramoorthy, A. S.; Lobo, R. F.; Vlachos, D. G. Coarse-Grained Models for Scale-Up of Structured Reactors. *Ind. Eng. Chem. Res.* **2025**, *64*, 14110−14121.
(11) Morais, E.; Delikonstantis, E.; Scapinello, M.; Smith, G.; Stefanidis, G. D.; Bogaerts, A. Methane coupling in nanosecond pulsed plasmas: Correlation between temperature and pressure and effects on product selectivity. *Chem. Eng. J.* **2023**, *462*, No. 142227.
(12) Akande, O.; Lee, B. Plasma steam methane reforming (PSMR) using a microwave torch for commercial-scale distributed hydrogen production. *Int. J. Hydrog. Energy* **2022**, *47*, 2874−2884.
(13) Akay, G.; Zhang, K.; Al-Harrasi, W. S. S.; Sankaran, R. M. Catalytic Plasma Fischer−Tropsch Synthesis Using Hierarchically Connected Porous Co/SiO_2 Catalysts Prepared by Microwave-Induced Co-assembly. *Ind. Eng. Chem. Res.* **2020**, *59*, 12013−12027.
(14) Mohamed, R. Y. A.; Kumarachari, R. K.; Bukke, S. P. N.; Neerugatti, D.; Mekasha, Y. T.; Bandarupalle, K. Plasma catalysis for sustainable industry: lab-scale studies and pathways to upscaling. *Discovery Appl. Sci.* **2025**, *7*, 271.
(15) Ceylan, S.; Friese, C.; Lammel, C.; Mazac, K.; Kirschning, A. Inductive Heating for Organic Synthesis by Using Functionalized Magnetic Nanoparticles Inside Microreactors. *Angew. Chem., Int. Ed.* **2008**, *47*, 8950−8953.
(16) Scarfiello, C.; Bellusci, M.; Pilloni, L.; Pietragiacomi, D.; La Barbera, A.; Varsano, F. Supported catalysts for induction-heated steam reforming of methane. *Int. J. Hydrogen Energy* **2021**, *46*, 134−145.
(17) Faure, S.; Kale, S. S.; Mille, N.; Cayez, S.; Ourlin, T.; Soulantica, K.; Carrey, J.; Chaudret, B. Improving energy efficiency of magnetic CO methanation by modifying coil design, heating agents, and by using eddy currents as the complementary heating source. *J. Appl. Phys.* **2021**, *129*, No. 044901.
(18) Teel, H.; Craps, M.; Mercado, H.-C.; Ciesielski, P.; Shimpalee, S. Numerical simulation for the design of induction heating based radio frequency reactor for ethylene production. *Chem. Eng. Res. Des.* **2025**, *219*, 511−521.
(19) Yan, Y.; Li, N.; Pan, Y.; Shi, L.; Xie, G.; Liu, Z.; Liu, Q. Hydrogen-rich syngas production from tobacco stem pyrolysis in an electromagnetic induction heating fluidized bed reactor. *Int. J. Hydrogen Energy* **2024**, *68*, 1271−1280.
(20) Kim, Y. T.; Lee, J.-J.; Lee, J. Electricity-driven reactors that promote thermochemical catalytic reactions via joule and induction heating. *Chemical Engineering Journal* **2023**, *470*, No. 144333.
(21) Wang, N.; Otor, H. O.; Rivera-Castro, G.; Hicks, J. C. Plasma Catalysis for Hydrogen Production: A Bright Future for Decarbonization. *ACS Catal.* **2024**, *14*, 6749−6798.
(22) Lucía, O.; Maussion, P.; Dede, E. J.; Burdío, J. M. Induction Heating Technology and Its Applications: Past Developments, Current Technology, and Future Challenges. *IEEE Transactions on Industrial Electronics* **2014**, *61*, 2509−2520.
(23) Zhao, Q.; Wu, F.; He, Y.; Xiao, P.; Webley, P. A. Impact of operating parameters on CO capture using carbon monolith by Electrical Swing Adsorption technology (ESA). *Chemical Engineering Journal* **2017**, *327*, 441−453.
(24) Deng, B.; Eddy, L.; Wyss, K. M.; Tiwary, C. S.; Tour, J. M. Flash Joule heating for synthesis, upcycling and remediation. *Nature Reviews Clean Technology* **2025**, *1*, 32−54.
(25) Mallapragada, D. S.; et al. Decarbonization of the chemical industry through electrification: Barriers and opportunities. *Joule* **2023**, *7*, 23−41.
(26) Noble, J. P. P.; Bending, S. J.; Hill, A. K. Radiofrequency Induction Heating for Green Chemicals Manufacture: A Systematic Model of Energy Losses and a Scale-Up Case-Study. *ACS Engineering Au* **2024**, *4*, 450−463.
(27) Rudnev, V.; Loveless, D.; Cook, R. L. *Handbook of Induction Heating*, 2nd ed.; CRC Press: Boca Raton, 2017; p 772.
(28) Ceylan, S.; Coutable, L.; Wegner, J.; Kirschning, A. Inductive Heating with Magnetic Materials inside Flow Reactors. *Chemistry − A. European Journal* **2011**, *17*, 1884−1893.
(29) Wang, W.; Tuci, G.; Duong-Viet, C.; Liu, Y.; Rossin, A. Induction Heating: An Enabling Technology for the Heat Management in Catalytic Processes. *ACS Catal.* **2019**, *9*, 7921−7935.
(30) Lin, C. H.; Wan, C.; Ru, Z.; Cremers, C.; Mohapatra, P.; Mantle, D. L.; Tamakuwala, K.; Hoffelmann, A. B.; Kanan, M. W.; Rivas-Davila, J.; Fan, J. A. Electrified thermochemical reaction systems with high-frequency metamaterial reactors. *Joule* **2024**, *8*, 2938−2949.
(31) Ambrosetti, M.; Bracconi, M.; Maestri, M.; Groppi, G.; Tronconi, E. Packed foams for the intensification of catalytic processes: assessment of packing efficiency and pressure drop using a combined experimental and numerical approach. *Chemical Engineering Journal* **2020**, *382*, No. 122801.
(32) Visconti, C. G.; Groppi, G.; Tronconi, E. Highly conductive "packed foams": A new concept for the intensification of strongly endo- and exo-thermic catalytic processes in compact tubular reactors. *Catal. Today* **2016**, *273*, 178−186.
(33) Eigenberger, G.; Ruppel, W. *Ullmann's Encyclopedia of Industrial Chemistry*; John Wiley & Sons, Ltd, 2012.
(34) Kapteijn, F.; Moulijn, J. A. Structured catalysts and reactors − Perspectives for demanding applications. *Catal. Today* **2022**, *383*, 5−14.
(35) Wang, Y.; Lucia, O.; Zhang, Z.; Gao, S.; Guan, Y.; Xu, D. A Review of High Frequency Power Converters and Related Technologies. *IEEE Open Journal of the Industrial Electronics Society* **2020**, *1*, 247−260.
(36) Lemlich, R. A theory for the limiting conductivity of polyhedral foam at low density. *J. Colloid Interface Sci.* **1978**, *64*, 107−110.
(37) Eom, J.-H.; Kim, Y.-W.; Raju, S. Processing and properties of macroporous silicon carbide ceramics: A review. *Journal of Asian Ceramic Societies* **2013**, *1*, 220−242.
(38) Sangsuwan, P.; Orejas, J. A.; Gatica, J. E.; Tewari, S. N.; Singh, M. Reaction-Bonded Silicon Carbide by Reactive Infiltration. *Ind. Eng. Chem. Res.* **2001**, *40*, 5191−5198.
(39) Gianella, S.; Gaia, D.; Ortona, A. High Temperature Applications of SiSiC Cellular Ceramics. *Adv. Eng. Mater.* **2012**, *14*, 1074−1081.
(40) *47 CFR Part 18 − Industrial, Scientific, and Medical Equipment.* **2025**. https://www.ecfr.gov/current/title-47/part-18 (accessed 2025−07−25).
(41) González-Castaño, M.; Dorneanu, B.; Arellano-García, H. The reverse water gas shift reaction: a process systems engineering perspective. *Reaction Chemistry & Engineering* **2021**, *6*, 954−976.

https://doi.org/10.1021/acssuschemeng.5c07929
ACS Sustainable Chem. Eng. 2026, 14, 5323−5331

(42) Li, C. S.; Frankhouser, A. D.; Kanan, M. W. Carbonate-catalyzed reverse water-gas shift to produce gas fermentation feedstocks for renewable liquid fuel synthesis. *Cell Reports Physical Science* **2022**, *3*, No. 101021.
(43) Tamakuwala, K. N.; Kennedy, R. P.; Li, C. S.; Mutz, B.; Boller, P.; Bare, S. R.; Kanan, M. W. Intermediate-Temperature Reverse Water−Gas Shift under Process-Relevant Conditions Catalyzed by Dispersed Alkali Carbonates. *JACS Au* **2025**, *5*, 1083−1089.
(44) Durlofsky, L.; Brady, J. F. Analysis of the Brinkman equation as a model for flow in porous media. *Phys. Fluids* **1987**, *30*, 3329−3341.

https://doi.org/10.1021/acssuschemeng.5c07929
ACS Sustainable Chem. Eng. 2026, 14, 5323−5331